Perturbed-angular-correlation study of the electric-field gradient in ^{181}Hf-doped and implanted indium sesquioxide

M. Rentería, F. G. Requejo, A. G. Bibiloni, A. F. Pasquevich, and J. Shitu
Departamento de Física, Facultad de Ciencias Exactas, Universidad Nacional de La Plata, CC N°67, 1900 La Plata, Argentina

K. Freitag
Institut für Strahlen- und Kernphysik der Universität Bonn, Nussallée 14-16, 5300 Bonn, Germany
(Received 31 July 1996; revised manuscript received 30 January 1997)

We studied the hyperfine interactions of ^{181}Ta in In_2O_3 by means of perturbed-angular-correlation (PAC) measurements. We prepared thin films of indium sesquioxide with different degrees of initial amorphism and implanted them with ^{181}Hf. Chemically prepared indium-sesquioxide powder samples were also made starting from neutron-irradiated $HfCl_4$, which provides the ^{181}Hf PAC probes. PAC experiments were performed on each sample at room temperature, after each step of annealing programs at increasing temperatures up to the full crystallization of the samples. The results indicate that the PAC probe occupies preferentially the axially symmetric cation site. Point-charge-model calculations were performed. The calculated asymmetry parameters η were compared with those obtained in ^{181}Hf PAC experiments performed also on other binary oxides, showing that the symmetry of the electric-field-gradient (EFG) tensor at ^{181}Ta cation sites in binary oxides is mainly determined by the nearest-neighbor oxygen-ion distribution around the probe. Comparisons of the experimental results in bixbyites obtained for both PAC probes, ^{111}Cd and ^{181}Ta, show that the local EFG in bixbyites, are strongly dependent on the geometry of the sites and the electronic configuration of the probes. [S0163-1829(97)01021-7]

I. INTRODUCTION

In recent years the development of methods for electron-density calculation in solids led to reliable predictions of electric-field gradients (EFG) in crystal lattice sites.[1] But, when the interest is focused on the EFG at the site of diluted impurities, a good enough theoretical approximation is not yet available that, at the same time, differentiates the contributions that give rise to the EFG in a solid. This is the case for first-principles methods, which in addition imply a considerable volume of calculation. In these concerns, the large number of experimental data of EFG measured at the site of the PAC impurity ^{111}Cd in binary oxides (see, for example, Refs. 2 and 3) has been object of analysis, in which investigators search for empirical correlations.[4,5]

Now, in PAC experiments, the second most commonly used radioactive probe is ^{181}Hf, which decays to ^{181}Ta. Tantalum has a quite different electronic configuration from that of cadmium and is a donor impurity in the majority of the binary oxides. The question of charge compensation becomes more important in the case of the hafnium probe due to the high oxidation state of Ta^{+5}. So, the extension of the mentioned analysis to this PAC impurity looks of interest. With that purpose, some time ago, we started a systematic study of one of the binary oxide group, i.e., the bixbyites, using ^{181}Ta as probe atom.[6,7] This group is quite interesting, since it includes rare and non-rare-earth cations and exhibits two inequivalent crystallographic sites for them, called C and D, with relative abundance 3:1. In effect, the cations form a nearly cubic, face-centered crystal lattice, in which six out of the eight tetrahedral sites are occupied by oxygen ions. Site D is axially symmetric and can be described as an In ion surrounded by six oxygen ions at the corners of a distorted cube, leaving two corners on the same diagonal free. In site C the cube is more distorted and the six oxygen ions leave two corners of a face diagonal free. Point-charge model (PCM) calculations yield asymmetry parameters η_D of 0.0 and η_C from 0.7 to 1.0.

One interesting result in the study of the behavior of the EFG in cation lattice sites in bixbyites is obtained when the relation of the quadrupole frequency corresponding to each site is displayed as a function of the host lattice constant a. The ratio ω_Q^C/ω_Q^D, using ^{111}Cd as probe, has been displayed in the a range 0.584–1.091 nm, i.e., from Sc to Sm sesquioxides. The obtained straight line accounts for a regular dependence. This figure, shown in Ref. 7, includes the results reported in that work for ^{181}Ta probes in Yb, Y and Dy sesquioxides as well as those for In_2O_3 taken from Ref. 6. These results lie on the same straight line, except for In_2O_3, which clearly departs from it. Therefore, at least in the region ranging from 1.043 nm for Yb sesquioxide to 1.065 nm for Dy sesquioxide, these results appear to show that both probes experience the same EFG relative strength between sites C and D.

The criteria used in the fits of Ref. 6 yield a 3:1 ratio between the fitted intensities of the hyperfine interactions (hi) associated to each cation site of the In_2O_3 crystal lattice. However, other fits could be obtained by using two hi that had almost the same χ^2. According to these fits, the ratio of the quadrupole frequencies lies on the mentioned straight line but the higher intensity corresponds to the hi produced by the probes located in the axially symmetric cation site, which is a minority in the crystal lattice.

Once we accept the inversion of the relative intensities,

the question arises whether it is caused by the initial degree of amorphism of the implanted sample or by the way in which the replacement of the cations by the hafnium probes, depending on the value of the lattice constant, takes place. In order to address this question a few experiments on samples with quite different initial state of amorphism were performed, i.e., radioactive hafnium was incorporated into a mixture of indium and hafnium chloride as described in Sec. II B 1 (completely amorphous sample), and implanted in a film with a major degree of crystallization than that of Ref. 6. Both samples were fully crystallized before the PAC measurements.

All the results we will present here, independently from the initial amorphism of the sample and the number of *hi* proposed to each fit, clearly show an inversion of the population of the cation sites *C* and *D* in In_2O_3: the ratio between populations of sites *C* and *D* is 1:2 or more distant from the stoichiometric relation 3:1. According to these results the relation between the quadrupole frequencies in this oxide lie on the straight line defined in Ref. 7. The experimental EFG tensors measured by PAC using ^{181}Ta as a probe isotope, for In_2O_3 and other binary oxides, are compared to PCM calculations including contributions from either the whole lattice or just the first nearest-neighbor (NN) oxygen ions. These results show that the EFG symmetry at ^{181}Ta sites in bixbyites could be mainly determined by the NN oxygen-ion distribution around the probe. The local EFG at ^{111}Cd and ^{181}Ta cation sites in bixbyites appear to be strongly correlated with both the geometry of the sites and the electronic configuration of the probe atom.

II. EXPERIMENTAL

A. Measurement technique and data reduction

The PAC technique is based on the determination of the influence of extra-nuclear fields on the correlation between emission directions of two successive radiations emitted during a nuclear-decay cascade. A complete description of this technique can be found in the literature.[8] We made use of the well-known 133–482 keV γ-γ cascade in ^{181}Ta, produced after the β^- nuclear decay of the ^{181}Hf$\rightarrow$^{181}Ta isotope. A conventional fast-slow coincidence system with four BaF_2 detectors in a coplanar 90° arrangement, with a time resolution of 0.9 ns, was used for data acquisition. Eight coincidence spectra, $C_{ij}(t)$, four taken between detectors positioned with 180° symmetry and four of eight possible with 90° symmetry, were simultaneously recorded in a 4-K memory multichannel analyzer. $C_{ij}(t)$ is the number of events in which the first γ ray enters detector *i* and, after a time *t*, the second enters detector *j*. The spectra, corrected for accidental counts, were combined to obtain

$$W(180°,t)=[C_{13}(t)+C_{31}(t)]^{1/2}[C_{24}(t)+C_{42}(t)]^{1/2} \quad (1)$$

and

$$W(90°,t)=[C_{12}(t)+C_{21}(t)]^{1/2}[C_{34}(t)+C_{43}(t)]^{1/2}. \quad (2)$$

Finally, the asymmetry ratio $R(t)$ becomes

$$R(t)=\frac{2[W(180°,t)-W(90°,t)]}{W(180°,t)+2W(90°,t)}\approx A_{22}^{\exp}G_{22}(t). \quad (3)$$

Theoretical functions of the form $A_{22}^{\exp}G_{22}(t)$, $A_{22}^{\exp}$ being the effective anisotropy of the cascade and $G_{22}(t)$ the perturbation factor

$$G_{22}(t)=\sum_i f_i\left[S_{20,i}+\sum_{n=1}^{3} S_{2n,i}\cos(\omega_{ni}t)e^{-\delta\omega_{ni}t}\right], \quad (4)$$

folded with the time resolution curve, were fitted to the experimental $R(t)$ asymmetry ratio. We denoted f_i the relative fractions of nuclei that experience a given perturbation. The ω_n frequencies are related to the quadrupole frequency $\omega_Q=eQV_{zz}/40\hbar$ by $\omega_n=g_n(\eta)\omega_Q$. The g_n and S_{2n} coefficients are known functions[9] of the axial-asymmetry parameter η, and the exponential functions in Eq. (4) account for a Lorentzian frequency distribution of relative width δ around ω_n.

B. Sample preparation and measurements

1. Sample I: Chemically prepared In_2O_3 (^{181}Hf) powder sample.

To obtain the ^{181}Hf-doped indium-sesquioxide, $HfCl_4$ with natural-isotopic-abundance hafnium was neutron irradi-

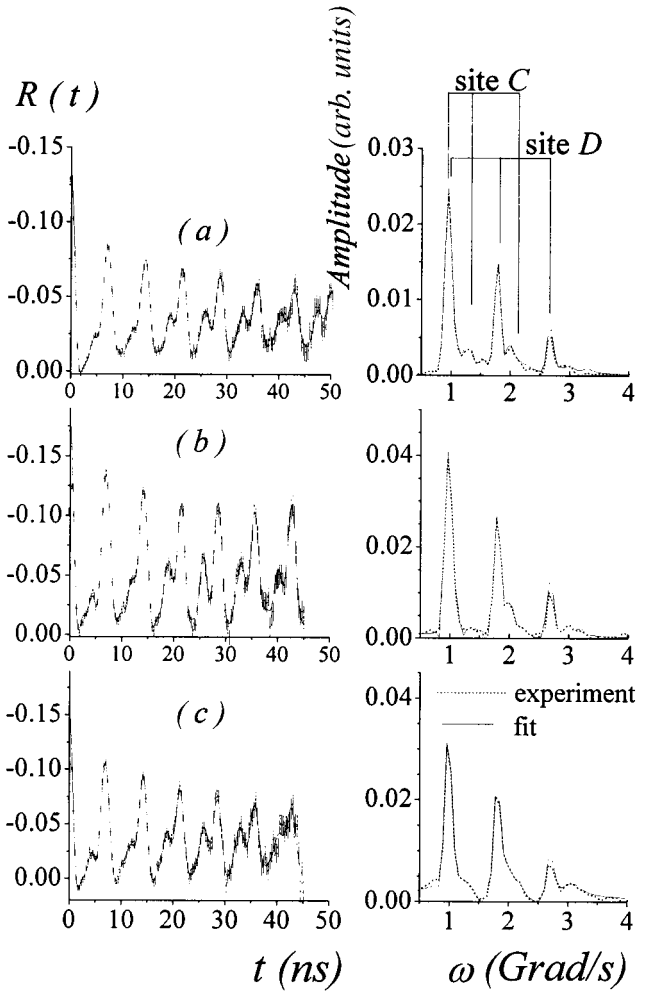

FIG. 1. PAC spectra (left) and Fourier spectra (right) measured at RT on: (a) chemically prepared In_2O_3(^{181}Hf) annealed 1 h at 1303 K, (b) ^{181}Hf-implanted ''crystalline'' In_2O_3 thin film annealed 1 h at 1273 K and (c) ^{181}Hf-implanted amorphous In_2O_3 thin film annealed 1 h at 1273 K (Ref. 6).

TABLE I. Hyperfine parameters obtained from least-squares fits of Eq. (4) to the spectra taken on the different samples displayed in Fig. 1.

Sample	Hyperfine interaction	f (%)	ω_Q (Mrad/s)	η	δ (%)
Chemically prepared	hi_1	45_2	146.2_2	0.149_7	0.8_1
	hi_2	35_8	110.7_8	0.6_9	9_1
	hi_3	12_2	163.9_6	0.05_7	1.9_7
	hi_4	8_1	161_2	0.84_2	3_1
Crystalline film	hi_1	61_2	147.0_1	0.150_6	0.4_1
	hi_2	9_2	115.3_7	0.54_2	0.9_9
	hi_3	25_3	164.3_5	0.14_2	2.0_5
	hi_4	5_1	157_1	0.84_2	0.1_8
Amorphous film	hi_1	61_4	146.5_2	0.157_7	1.1_2
	hi_2	8_3	107.5_6	0.75_2	0_1
	hi_3	19_6	164_1	0.18_3	3_1
	hi_4	12_2	158_2	0.66_3	3_1

ated to obtain ^{181}Hf from the reaction ^{180}Hf(n,γ)^{181}Hf with cross section $\sigma_\gamma = 13.0$ b for thermal neutrons. Then, 560 mg of indium and 15 mg of the irradiated $HfCl_4$ were dissolved in HNO_3. This solution was dropped into NH_4 (OH) at a rate of approximately 0.6 ml/min. The yellow gel precipitate was washed three times with water, then dried and calcined at 1373 K for a couple of hours. After calcination, the yellow powder turn into a pale green-blue powder. The final Hf concentration was about 1 at. % of In.

PAC measurements at room temperature (RT) in air were taken on the ''as prepared'' sample immediately after the 1373 K thermal treatment and after a 10 day series of 24-h PAC measurements at increasing temperatures in the range 446–1303 K. The PAC spectra taken at these temperatures showed that the quadrupole frequencies decrease with temperature as found also in the implanted thin-film samples. The last spectrum taken at RT was essentially equal to the ''as prepared'' sample spectrum, showing the reversibility of the process involved.

2. Sample II: ^{181}Hf-implanted In_2O_3 thin film.

An In-O thin film was prepared by thermal evaporation of high-purity In ($5N$) onto a rectangular alumina substrate, in a vacuum chamber where, after air evacuation, a flux of pure oxygen was introduced and kept at a pressure of about 2×10^{-3} Torr. The rectangular plate was kept at about 300 K and the thickness of the film was estimated to be 200 nm. After this procedure, the film received a thermal treatment of 1 h in air at 673 K, in order to obtain a more crystalline In_2O_3 film than that used in Ref. 6. With this annealing, the color of the film changed from black to vivid yellow. We used a not completely crystallized target since it is well known that thermal annealing treatments and phase transitions in oxides, following ion implantation, favor the replacement of host cations by PAC probes. In effect, when an impurity-implanted oxide reach its final crystalline phase and the radiation damage has been annealed, most of the probes are found on substitutional defect-free sites (see, for example, Refs. 10–12).

The ion accelerator facility of the Institut für Strahlen- und Kernphysik (ISKP, Bonn) was then used to implant $^{181}Hf^+$ ions into the annealed samples with energies of 150 keV and a dose of 10^{13} ions/cm^2. After implantation, the films received a series of isochronal (1 h) annealing treatments in air between 674 and 1273 K, in 100 K steps. The initial vivid yellow film turned into a pale yellow after 973 K, and became fully transparent after the 1273 K treatment.

PAC measurements were performed at RT in air after implantation and after each annealing treatment. The complete crystallization and radiation damage annealing was reached after the 1173 K thermal treatment. No change in the hyperfine interaction parameters was found after this annealing.

Below we refer to sample I as the ''chemical'' sample and to sample II as the ''crystalline'' one.

III. RESULTS AND PAC SPECTRA ANALYSIS

Figure 1 shows the experimental $R(t)$ and Fourier spectra, left and right, respectively, for ^{181}Ta in the chemically prepared In_2O_3 powder sample [Fig. 1(a)], in the ^{181}Hf-implanted ''crystalline'' thin film [Fig. 1(b)] and in the ^{181}Hf-implanted amorphous thin film [Fig. 1(c)] from Ref. 6, all taken at RT in air after the 1303 K thermal annealing treatment in the case of the ''chemical'' sample and the 1273 K treatment in the case of the films. At this point, all the samples have the highest fraction of probe nuclei located in well defined sites in the In_2O_3 lattice, as can be seen from the nearly undampened $R(t)$ spectra. A model that represents up to four well defined hyperfine interactions (hi) was needed to reproduce the experimental spectra. Full lines in Fig. 1 show the very good agreement between the experimental results and the $G_{22}(t)$ values obtained by least-squares fits of Eq. (4) to the data. The corresponding fitted parameters are shown in Table I. Let us now analyze separately the results obtained for each sample.

A. Chemically prepared In_2O_3 (^{181}Hf)

Figure 2 shows two fitted Fourier spectra (full lines) superimposed to those corresponding to the experimental data (dotted lines). These data were taken at RT after the sample underwent a program of 24 h thermal treatments in air at

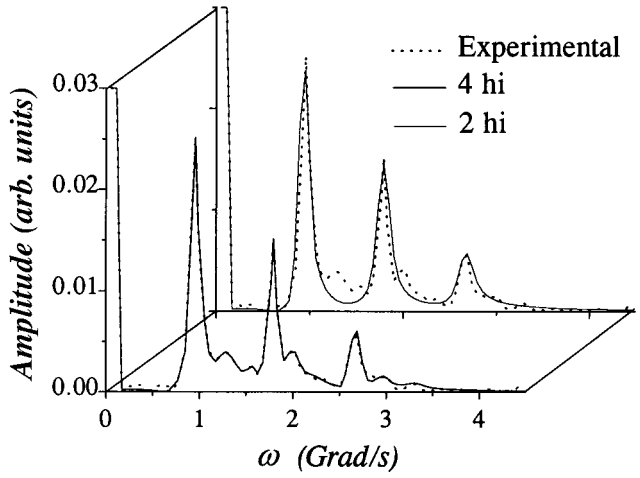

FIG. 2. Fitted spectra with two (narrow line) and four (wide line) hyperfine interactions superimposed to the experimental Fourier spectrum taken on the ''chemical'' sample at RT after the annealing at 1373 K (dotted lines).

temperatures from 446 to 1303 K in approximately 100 K steps (10 days of cumulative annealing) following an initial 2-h treatment at 1373 K. Full lines correspond to Fourier spectra obtained from fits with two (narrow line) and four (wide line) hyperfine interactions. It is clear that, while the fit with four hi reproduces quite well the experimental data, the other fit not only has a low quality but even cannot reproduce some of the experimental peaks. To emphasize this assertion Fig. 3 shows separately the result for each of the four interactions proposed. Each one corresponds to peaks in the experimental spectrum, all them being necessary. The fitted parameters of the four components are displayed in Table I. It can be mentioned that fits on a spectrum taken immediately after the initial treatment at 1373 K yield the same parameters. The strongly populated hi (hi_1 and hi_2) correspond to the peaks pointed out in the Fourier spectrum in Fig. 1(a). Two weakly populated hi (hi_3 and hi_4) were also needed, to account for the rest of the peaks.

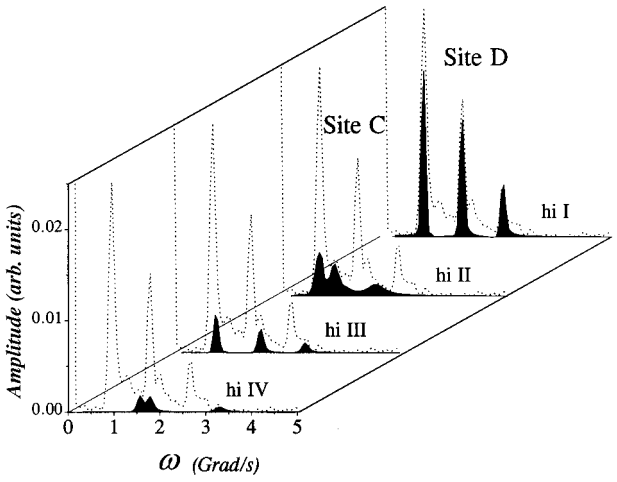

FIG. 3. Each of the four hyperfine interactions fitted in the spectrum shown in Fig. 2 are displayed separately. The relative intensities of each hi have been taken into account.

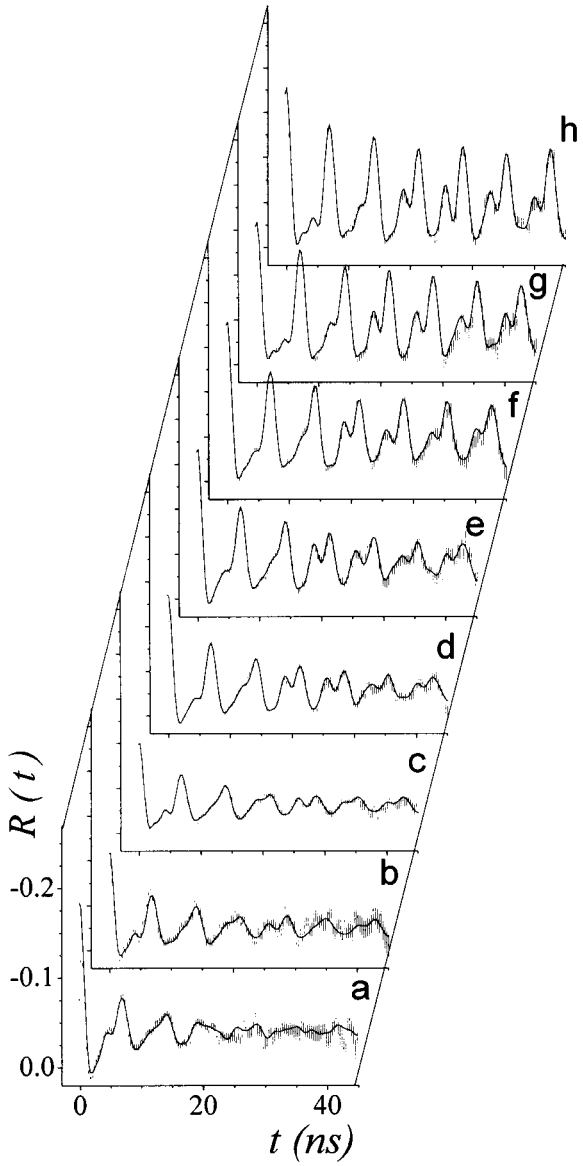

FIG. 4. PAC spectra measured at RT on the ^{181}Hf-implanted ''crystalline'' In_2O_3 thin film after each of the following 1 h annealing treatments, reflecting different degrees of crystallinity in the sample: (a) as implanted, after the initial 673 K treatment, (b) 673 K, (c) 773 K, (d) 873 K, (e) 973 K, (f) 1073 K, (g) 1173 K, and (h) 1273 K.

B. ^{181}Hf-implanted In_2O_3 thin films

Different experiments were performed in this case. Figure 4 shows the experimental PAC results obtained on the ''crystalline'' sample. This figure shows the complete series of PAC spectra taken on this film at RT after each 1 h annealing treatment indicated in the caption. This plot displays the evolution of the $R(t)$ pattern that characterizes different stages of crystallization (suggested by the removal of the damping of the spectra) and probe occupation of both cationic sites. Figure 5 shows the PAC spectra taken at RT on the sample of Ref. 6 after each step of a similar program of annealing treatments. This sequence, not shown in Ref. 6, reflects the difference in the sample preparation. The similarity between

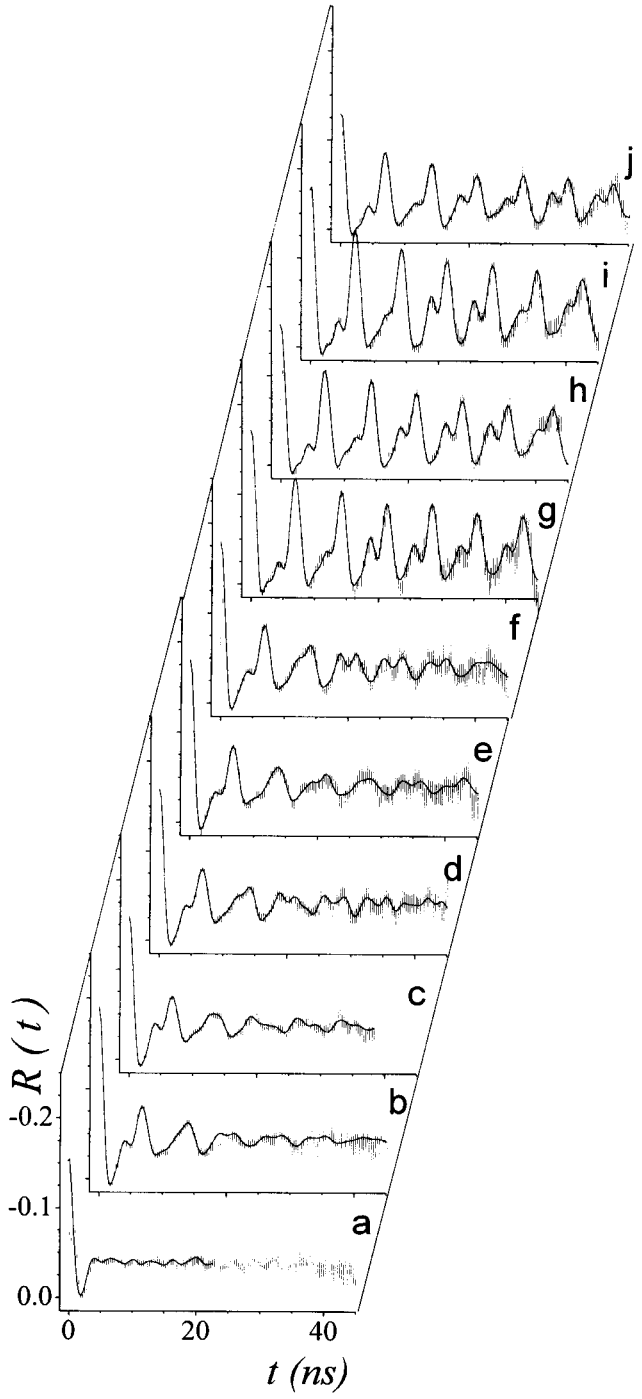

FIG. 5. PAC spectra measured at RT on the ^{181}Hf-implanted amorphous In_2O_3 thin film (Ref. 6) after each of the following 1 h annealing treatments: (a) as implanted, immediately after evaporation, (b) 473 K, (c) 573 K, (d) 673 K, (e) 773 K, (f) 873 K, (g) 973 K, (h) 1273 K, (i) 1373 K , and (j) 1473 K.

the first spectrum in Fig. 4 and the spectra labeled (c) and (d) in Fig. 5 confirms the major initial degree of crystallization of the ''crystalline'' sample.

The full lines in Figs. 4 and 5 represent the results of the least-squares fits with four hyperfine interactions. Figure 6 shows the behavior of the values of ω_Q, η, and δ resulting for hi_1 and hi_2 as function of the annealing temperature.

The results obtained in the experiments with the films are less defined than those obtained in the case of the ''chemical'' sample. The smoothness of the Fourier spectra, as Figs. 1(b) and 1(c) show, makes it difficult to correlate each hi component with the peaks in the spectra.

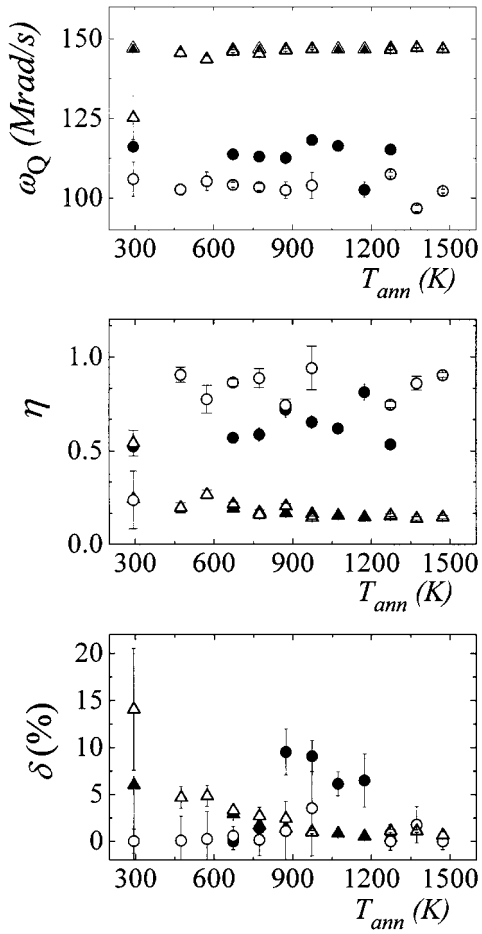

FIG. 6. Evolution of the hyperfine parameters ω_Q, η, and δ for hi_1 and hi_2 obtained with the film samples (see text) as function of the annealing treatment temperature. Black triangles (site D) and circles (site C) denote data coming from the ''crystalline'' sample ; open triangles (site D) and circles (sites C) data coming from the amorphous sample.

IV. DISCUSSION

In Table I we showed a consistent set of hyperfine parameters that fits the PAC patterns of the three samples studied. We will center our discussion on the assignment of the hyperfine interactions that present the higher intensity and are associated to sites C and D in the bixbyite structure of In_2O_3. Since according to our assignment the relative population of probes in site C will be lower than that of site D, we will discuss this briefly in terms of the crystal chemistry of the bixbyites, i.e., in terms of the local charge density and the size of the sites. Then we will give some possible interpretation for the other two hi we fitted. Finally, we will make use of the whole set of ^{181}Ta PAC measurements in binary oxides in order to study a possible correlation between the experimental asymmetry parameter η and the symmetry of the nearest-neighbor oxygen ions around the ^{181}Ta nucleus. The EFG results at both ^{111}Cd and ^{181}Ta

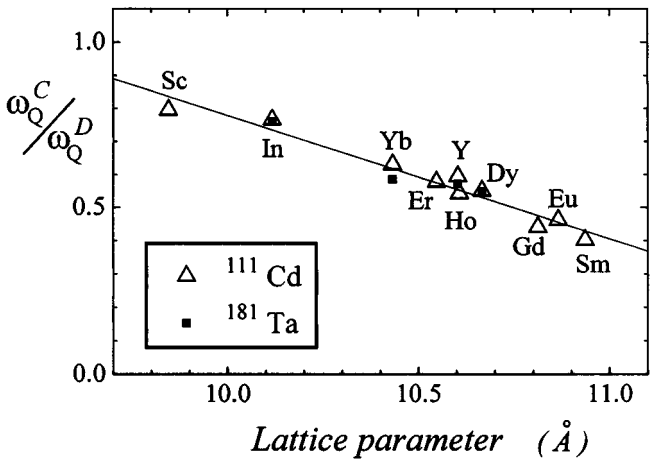

FIG. 7. Ratio of the quadrupole frequencies of site C to that of site D in bixbyites coming from PAC measurements using ^{111}Cd (open triangles) and ^{181}Ta (black squares) as probes. Solid line: linear fit to all the data. The errors in the ^{111}Cd and ^{181}Ta data are less than 0.01 and 0.008, respectively, and are largely included in the size of the symbols. Note that in the case of In_2O_3 the results for both probes are coincident.

cation sites in bixbyites will be compiled and studied in the frame of the semiempirical model we developed for ^{111}Cd,[4] in order to extract information about the influence of the electronic configuration of the probe atoms on the local electric-field gradient in these compounds.

Let us discuss first the assignment of hi_1 and hi_2 that amount more than 70% of the total intensity. According to the symmetry of the two sites we expect $\omega_Q(D) > \omega_Q(C)$ and $\eta_D < \eta_C$. So, if we assign $hi1$ to site D and $hi2$ to site C, both conditions are fulfilled. Furthermore, the ratio of the quadrupole frequencies of these two interactions is coincident with that found for the corresponding interactions of ^{111}Cd in In_2O_3 and both lie on the same straight line shown sin Fig. 7. This should confirm the existence of a regular dependence of this ratio on the lattice parameter a. We will return to this point at the end of this section.

The well defined hi assigned to site D was found in all the samples. This shows the total crystallization of the samples. However, some features of the evolution of the hi of site C show that the process of crystallization in each sample in the microsurroundings of this site is not exactly the same. In effect, comparing the EFG distribution δ for the two films (see Fig. 6) we can see that δ_C for the amorphous film is always smaller than that corresponding to the ''crystalline'' film along the crystallization process. This fact supports the idea that the doping of the impurity prior to the crystallization of site C, which exhibits a difficulty to be populated by ^{181}Hf ions, probably favored the complete crystallization of the neighborhood of the site. This situation could be hindered in the ''chemical'' sample by the defects originated in the higher level of impurities it has.

As we mentioned above, the main fraction of tracers in the PAC experiment is located in the axially symmetric cation environment in bixbyites. Considering the crystal chemistry of the bixbyites, i.e. the local charge density and the sizes of the sites, with and without the impurity, some possible explanations arise. The evaluation of the electrostatic potential at each site in In_2O_3, considering the ionic contribution up to the nearest-neighbor cations, yields a higher positive potential for site D (6.62 nV) compared to that obtained for site C (6.33 nV), resulting in the D site being a less attractive environment for a positive ion. If only the NN oxygen ions are considered, the results show again that site C represents a more attractive environment for a cation. This rule also applies to all the bixbyites.

These calculations do not include the possible effect of the charge excess of the Hf^{4+} impurity on the local charge density at sites C and D. However, it is possible to evaluate in a very simple way whether the charge state of the impurity introduces or not any difference when it replaces an In ion of sites C or D. Considering the empirical expression proposed by Brown and Wu[13] for calculating cation-oxygen bond valences:

$$S = \frac{R}{R_1}^{-N}, \tag{5}$$

where S and R are the bond valence and bond length of a cation-oxygen bond in a certain cation-oxygen cluster, we can estimate the bond valence at sites C and D with In^{3+} and Hf^{4+} as central atoms. In Eq. (5), R_1 and N are empirical parameters related to the central cation properties (namely electronic configuration and oxidation state of the central atom). Using the empirical parameters for In^{3+} and Hf^{4+} reported in Ref. 13 and the atomic positions quoted in Ref. 14 for In_2O_3, the bond valence calculated with Eq. (5) should generate also a more attractive potential at site C than that of site D when In^{3+} is considered as the central atom. However, the difference between the electrostatic potential at these sites is smaller in approximately 30% when a Hf^{4+} ion replaces the In ion. This fact could favor the preferential occupancy of site D; especially if another additional effect such as cation sizes contributes in the same way. It seems that this is what occurs for sesquioxides with lattice parameters smaller than that of Dy sesquioxide. Figure 8 plots the cation-oxygen distances for sites C and D, for all the bixbyites measured with ^{111}Cd, as function of the lattice parameter a. In these structures, the length of the six bonds at site D is equal, while site C presents three pairs of different bond lengths. Figure 8 shows that as a becomes smaller the available size in site D becomes larger with respect to that of site C. The horizontal straight lines in this figure represent the seven cation-oxygen bond lengths of the Hf ion in m-HfO_2, the natural and stable phase of hafnium oxide.[15] It is clear that for bixbyites with lattice parameter smaller than that of Yb sesquioxide the available space in site C becomes smaller than the ideal mean space for Hf in its oxide. This can be the reason why an inversion in the lattice sites population has only been seen in In_2O_3 [preliminary PAC results show the same behavior in Sc_2O_3(^{181}Ta) (Ref. 16)].

The low EFG distribution of hi_3 and hi_4 ($\delta < 4\%$) could merit some comments about their possible origins, although they represent just 20–30 % of the total intensity and do not satisfy the same arguments used to assign hi_1 and hi_2 to probes located in regular lattice sites.

A possible configuration in agreement with these results is obtained when a ^{181}Ta probe in site D has a Hf ion located as next-near neighbor (NNN). If the Hf concentration rises

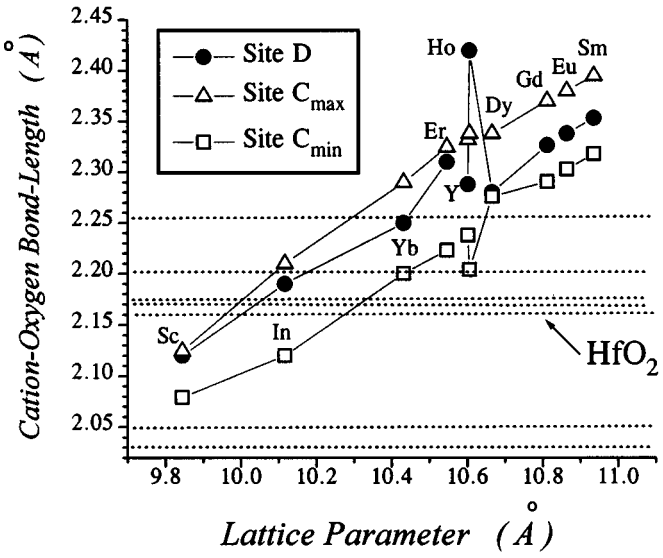

FIG. 8. Cation-oxygen bond length of all the bixbyites measured with ^{111}Cd as function of the lattice parameter of each sesquioxide. Only the minimun and maximun cation-oxygen distances for site *C* are shown for simplicity. The horizontal dotted lines represent the seven Hf-O bond lengths in *m*-HfO_2.

up to around 1 at.% of In, as is the case of the chemical sample, this situation leaves about, at least, 5% of the probe ions with this type of defect. A certain lack of homogeneity in the samples preparation could produce zones with a major density of Hf ions. In effect, this type of defect configuration gives rise to only two inequivalent EFG, depending on which of the 12 NNN ions is replaced. Predictions within the PCM for these NNN configurations, taking into acount the whole lattice, reproduce almost exactly the hyperfine parameters displayed in Table I for hi_3 and hi_4, i.e., not only the absolute values of η but also the relative strength between the EFG at ^{181}Ta in site *D*, with and without the defect. The calculations of the EFG tensor for this type of defect around the asymmetric site *C* predict six different quadrupole frequencies that should give rise to a quadrupole frequency distribution of about 10–15 %, in excellent agreement with the distribution δ_C found for site *C* in the ''chemical'' sample (see Table I). Therefore, the presence of Hf impurities as NNN of a Ta ion in site *D* yield two additional interactions hi_3 and hi_4, while a similar situation around site *C* contributes to a larger quadrupole frequency distribution of hi_2. This distribution could be hindering the complete crystallization of site *C* in the mentioned sample.

The asymmetric site *C* in bixbyites is one of the few cases among the binary oxides where the PCM prediction of the asymmetry parameter arising from the NN oxygen contribution, $\eta^{\rm NN}$, and from the whole lattice, $\eta^{\rm latt}$, are not equal. Therefore, these crystallographic site is a good candidate to check the assumption that the EFG symmetry in ^{181}Ta cation sites is correlated with the symmetry of the nearest-neighbor oxygen ions. The PCM predicts for In_2O_3 an asymmetry parameter $\eta_D^{\rm latt}=0.0$ and $\eta_C^{\rm latt}=0.84$ for the lattice contribution, in overall agreement with the values shown in Table I. The asymmetry parameter prediction for site *C* in In_2O_3 becomes smaller ($\eta_C^{\rm NN}=0.55$) if only the nearest-neighbor oxygen ions are considered in the calculation of the V_{ij} tensor. This value is closer to the experimental asymmetry parameter $\eta_C^{\rm exp}$ than the value $\eta_C^{\rm latt}$ predicted by the complete lattice contribution. All the experimental EFG-tensor results at ^{181}Ta sites in binary oxides, in those cases where $\eta^{\rm NN} \neq \eta^{\rm latt}$, show also a similarity between $\eta^{\rm exp}$ and $\eta^{\rm NN}$. A possible explanation based on the contribution of the local electrons in the neigborhood of the probe is the following. From a systematic study of the EFG at ^{111}Cd in binary oxides we know that the strength of the lattice and NN contributions to the V_{zz} component of the EFG tensor in binary oxides have the same order of magnitude, but they are both negligible compared to the local contribution.[4,5,17] This behavior also applies to the case of the ^{181}Ta PAC probe.[18] Therefore, the similarity between $\eta^{\rm exp}$ and $\eta^{\rm NN}$ could imply that the electric-field-gradient symmetry at ^{181}Ta in binary oxides is mainly determined by the symmetry of the nearest-neighbor oxygen-ion distribution, which imposes its symmetry on the local electron distribution around the probe atom.

The results obtained in the present work for In_2O_3 show that the ratio ω_Q^C/ω_Q^D for both ^{111}Cd and ^{181}Ta probe nuclei are coincident, as Fig. 7 displays. This is true in the range of the lattice parameter *a* corresponding from In to Dy sesquioxides. The slope of the lines shown in Fig. 7 clearly differs from the mean value of 0.5 predicted by the PCM for that ratio in all the bixbyites.[7]. This is not surprising since the local EFG contribution is not included in that calculation. In the frame of the semiempirical model we developed to describe the different contributions to the EFG at ^{111}Cd cation sites in binary oxides,[4,5] the quadrupole frequency measured at site *i* with a certain *probe* can be described as

$$\omega_Q^{\rm probe}({\rm Site}\ \ i) \propto (1-\mu)^{{\rm Site}\ \ i,{\rm probe}}(1-\gamma_\infty)^{\rm probe} V_{zz}^{\rm lattice}({\rm Site}\ \ i), \tag{6}$$

where γ_∞ is the Sternheimer factor[19] of the probe and $V_{zz}^{\rm lattice}$(Site *i*) is the EFG lattice contribution at site *i*. The antishielding factor (1-μ) is attributed to the local EFG produced by semicore and valence electrons of the probe atom and its nearest neighbors. In Refs. 4,5 the dependence of the μ factor with the geometry of the site was clearly shown. In Ref. 18 a similar empirical correlation with a different slope showed that this factor could depend also on the probe used. If Eq. (6) is applied to describe the ratio ω_Q^C/ω_Q^D shown in Fig. 7, the coincidence of the data for both probes appears to show that the ratio $(1-\mu)^{{\rm Site}\ C}/(1-\mu)^{{\rm Site}\ D}$ does not depend on the probe used. This statement is not true. In effect, the experimental ratio $\omega_Q^{\rm Ta}({\rm Site}\ \ i)/\omega_Q^{\rm Cd}({\rm Site}\ \ i)$ yields values for In_2O_3 that do not depend on the site considered. This is also verified for Yb, Y, and Dy sesquioxides, as previously shown in Ref. 7. But, in these cases, the experimental ratio also show that the ratio $(1-\mu)^{{\rm Ta,Site}\ i}/(1-\mu)^{{\rm Cd,Site}\ i} \neq 1$. This means that the factor μ does not depend only on the geometry of the site but also on the electronic configuration of the probe. The apparent contradiction could be resolve if the antishielding factor μ could be factorized in two parts: one which depends mainly on the geometry of the sites and another that depends on the electronic configuration of the probes (like the core antishielding factor γ_∞ does).

V. CONCLUSIONS

We characterized the hyperfine interactions of ^{181}Ta in In_2O_3 in samples prepared by different methods. The results indicate that in all the cases the hafnium probes locate preferentially at the less abundant crystallographic site of the two inequivalent cation sites in bixbyites. This result seems to be independent of the initial state of amorphism of the sample. The available space in the lattice for the Ta probes seems to play an essential role for this preference.

Point-charge model calculations were performed with respect to the asymmetry parameter η for both cation sites in In_2O_3. The values predicted by just the contribution of the nearest-neighbor oxygen ions agree much better with the experiment than those obtained when all the crystal lattice is considered. This fact coincides with a tendency found in PAC measurements with ^{181}Ta in other binary oxides and could imply that the electric-field-gradient symmetry at ^{181}Ta sites in binary oxides is mainly determined by the nearest-neighbor oxygen-ion distribution around the probe. In particular, the local electric-field-gradient contribution at ^{111}Cd and ^{181}Ta sites in bixbyites shows a strong dependence on the geometry of the site and the electronic configuration of the probes.

ACKNOWLEDGMENTS

This work was performed within the framework of Programa TENAES of the Consejo Nacional de Investigaciones Científicas y Técnicas (CONICET), Argentina; partially supported by Comisión de Investigaciones Científicas de la Provincia de Buenos Aires (CICPBA), Fundación Antorchas, Argentina, Kernforschungs Zentrum Karlsruhe, Alexander von Humboldt Stiftung and Volkswagen Werkstiftung, Germany.

[1] P. Blaha, K. Schwarz, and P.H. Dederichs, Phys. Rev. B **37**, 2792 (1988); P. Blaha, P. Sorantin, C. Ambrosch, and K. Schwarz, Hyperfine Interact. **51**, 917 (1989); P. Blaha, D.J. Singh, P.I. Sorantin, and K. Schwarz, Phys. Rev. B **46**, 1321 (1992); P. Blaha, P. Dufek, K. Schwarz, and H. Haas, Hyperfine Interact. **97/98**, 3 (1996).

[2] D. Wiarda, M. Uhrmacher, A. Bartos, and K.P. Lieb, J. Phys. Condens. Matter **5**, 4111 (1992).

[3] J. Shitu, D. Wiarda, T. Wenzel, M. Uhrmacher, K.P. Lieb, S. Bedi, and A. Bartos, Phys. Rev. B **46**, 7987 (1992).

[4] M. Rentería, C.P. Massolo, and A.G. Bibiloni, Mod. Phys. Lett. B **6**, 1819 (1992).

[5] R. Weht, G. Fabricius, M. Weissmann, M. Rentería, C.P. Massolo, and A.G. Bibiloni, Phys. Rev. B **49**, 14 939 (1994).

[6] J.A. Vercesi, A.G. Bibiloni, C.P. Massolo, M.S. Moreno, A.F. Pasquevich, and K. Freitag, Phys. Rev. B **47**, 490 (1993).

[7] A.F. Pasquevich, A.G. Bibiloni, C.P. Massolo, M. Rentería, J.A. Vercesi, and K. Freitag, Phys. Rev. B **49**, 14 331 (1994).

[8] See, for example, H. Frauenfelder and R.M. Steffen, in *Alpha-, Beta-, and Gamma-Ray Spectroscopy*, edited by K. Siegbahn (North-Holland, Amsterdam, 1966), pp. 997 and 1182.

[9] L.A. Mendoza-Zélis, A.G. Bibiloni, M.C. Caracoche, A. López-García, J.A. Martínez, R.C. Mercader, and A.F. Pasquevich, Hyperfine Interact. **3**, 315 (1977).

[10] W. Bolse, M. Uhrmacher, and J. Kesten, Hyperfine Interact. **35**, 931 (1987).

[11] A. Bartos, W. Bolse, K.P. Lieb, and M. Uhrmacher, Phys. Lett. A **130**, 177 (1988).

[12] M. Rentería, A.G. Bibiloni, M.S. Moreno, J. Desimoni, R.C. Mercader, A. Bartos, M. Uhrmacher, and K.P. Lieb, J. Phys. Condens. Matter **3**, 3625 (1991).

[13] I.D. Brown and K.K. Wu, Acta Crystallogr. B **32**, 1957 (1976).

[14] M. Marezio, Acta Crystallogr. **20**, 723 (1966).

[15] R. Ruh and P.W.R. Corfield, J. Am. Ceram. Soc. **53**, 126 (1970).

[16] M. Rentería *et al.* (unpublished).

[17] M. Rentería, Ph.D. thesis, Departamento de Física, Facultad de Ciencias Exactas, Universidad Nacional de La Plata, 1992.

[18] M. Rentería (unpublished).

[19] F.D. Feiock and W.R. Johnson, Phys. Rev. **187**, 39 (1969). In the case of Ta^{5+}, the value came from interpolation between the Hf^{4+} and W^{6+} values.